Micromechanical investigation of granular ratcheting using a discrete model of polygonal particles

F. Alonso-Marroquín and H. B. Mühlhaus

Earth Systems Science Computational Centre, The University of Queensland, Sta. Lucia Qld 4068, Australia

H. J. Herrmann

Institut für Baustoffe, ETH-Höenggerberg, Zürich, Switzerland

Abstract

We use a two-dimensional model of polygonal particles to investigate granular ratcheting. Ratcheting is a long-term response of granular materials under cyclic loading, where the same amount of permanent deformation is accumulated after each cycle. We report on ratcheting for low frequencies and extremely small loading amplitudes. The evolution of the subnetwork of sliding contacts allows us to understand the micromechanics of ratcheting. We show that the contact network evolves almost periodically under cyclic loading as the subnetwork of the sliding contacts reaches different stages of anisotropy in each cycle. Sliding contacts lead to a monotonic accumulation of permanent deformation per cycle in each particle. The distribution of these deformations appears to be correlated in form of vortices inside the granular assembly.

Key words: Granular systems, Dynamics and kinematics of rigid bodies, Molecular dynamics methods
PACS: 45.70.-n, 45.40.-f, 47.11.Mn

1 Introduction

The existence of granular ratcheting as a long-time behavior in granular materials is still under discussion in the scientific and engineering community. This behavior refers to the constant accumulation of permanent deformation

per cycle, when the granular sample is subjected to loading-unloading stress cycles with amplitudes well bellow the yield limit [1]. Ratcheting regimes are observed in both numerical [2–6] and physical [7,8] experiments. There is no controversy about the existence of ratcheting when the stress amplitudes reach the yield criterion. However, it is not clear whether this effect persists for loading amplitudes well inside the yield surface, or whether there is a certain regime where no accumulation of deformation occurs. Numerical simulations have suggested that ratcheting may persist for loading amplitudes bellow the yield limit [2,6]. Here we investigate the microscopic origin of this effect, and how it affects the global deformation of the sample. We present numerical evidence of granular ratcheting for small loading amplitudes in the quasistatic regime.

This paper is organized as follows: In the Section 1.1 we introduce the concept of ratcheting, which has been used in recent year in many different contexts. In Section 1.2 we introduce two different types of constitutive models (hypoplastic and elastoplastic models) for modeling cyclic loading. In Section 1.3 we summarize recent micromechanical observations showing deviations from the *classical* soil mechanics and supporting the existence of the granular ratcheting regime. In Section 2 we study the long-time, quasistatic strain response of a dense polygonal packing under cyclic loading. A micromechanical investigation of granular ratcheting in terms of induced anisotropy and deformation patterns is presented in Section 3.

1.1 What is Ratcheting?

Chapter 46 of the Feynman Lectures on Physics [9] contains a celebrated illustration of ratcheting device. As shown in Fig. 1, the ratchet consist of a pawl that engages the sloping teeth of a wheel, permitting motion in one direction only. In Feynman's ratchet, an axle connects this wheel with some vanes, which are surrounded by a gas. The vanes are randomly hit by the gas molecules, but due to the presence of the pawl, only collisions in one direction can make the wheel lift the pawl and advance it to the next notch.

The possibility to extract work from noise using such ratchet devices has attracted interest from many researchers [10–12]. Brownian motors, quantum ratchets or molecular pumps, all these machines operates under a similar ratcheting mechanism: The chaotic Brownian motion of the microworld cannot be avoided, but one can take advantage of it [12]. There is an extensive body of work on this subject, driven by the need to understand the molecular motors that are responsible for many biological motions, such as cellular transport [13] or muscle contraction [14]. Recently, this kind of mechanism has been experimentally demonstrated using the technology available to build microm-

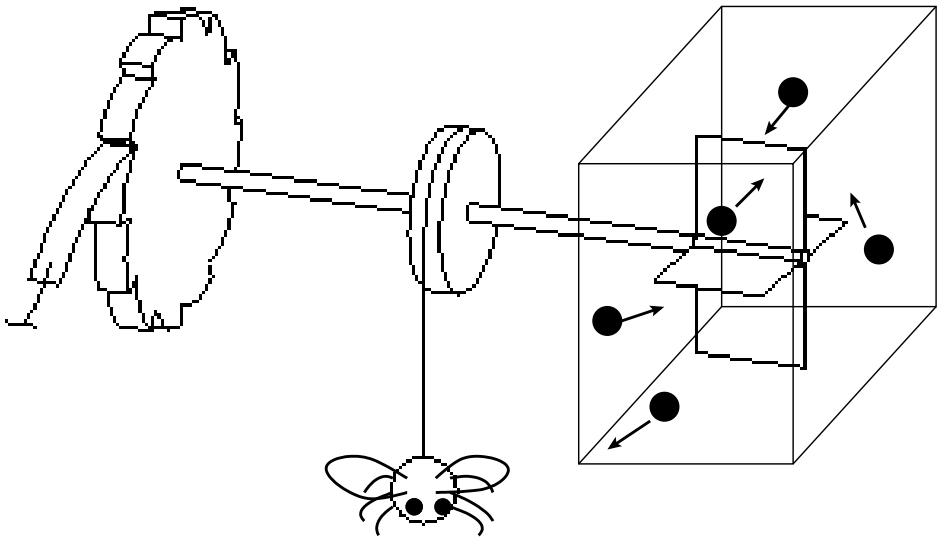

Fig. 1. Microscopic ratchet device introduced by Feynmann [9]. A wheel that can only turn one way is connected to a vane by an axle. The vane is inside a box with gas molecules in thermal equilibrium. Molecules randomly hit the vane. The sloping teeth of the wheel rectify the motion. The whole device converts random motion in work that can be used to lift a fly.

eter scale structures. Many man-made ratchet devices have been constructed, and they are used as mechanical and electrical rectifiers [12]. Apart from these fascinating machines, the ratchet effect is used to describe economical or sociological processes where the intrinsic asymmetry in the system allows rectification of an unbiased input [15]. In geological materials, ratcheting is a major cause of deterioration when the material is subjected to cyclic loading, thermal or mechanical fluctuations [8,16,17]. An asymmetry in a foundation can produce tilting and eventual collapse of an engineering structure due to ratcheting [18]. The tower of Pisa [19] is a well documented structure, where the tilt has been observed from its construction in 1174. Railway design is another important example. Granular materials are used as a supportive railbed. The excitations caused by trains induces permanent deformation in the granular bed [20]. Therefore a better understanding of the ratcheting response will reduce the maintenance cost of many engineering structures.

1.2 Constitutive modeling

The modeling of the cyclic loading behavior of soils has been a central issue in the development of advanced constitutive equations. The 1960s have seen many significant developments in this field. Prior to this, soil mechanics was

confined to linear elastic theory and the Mohr-Coulomb failure criterion. An important advance in the scope of soil plasticity occurred after the pioneering work of Roscoe and his coworkers in Cambridge, which led to the basic principles of the Critical State Theory [21,22]. In an attempt to cover further aspects of cyclic soil behavior, subsequent developments have given rise to a great number of constitutive models [23].

One important result of the theory of plasticity is the so-called *shakedown theory* [24–27]. This theory predicts that a granular material accumulates plastic strains under cyclic loading if the magnitude of the applied load exceeds a threshold value called the shakedown limit. The material is then said to exhibit *incremental collapse* or *ratcheting*. If the loads are below this threshold, the accumulation of permanent deformation stops after a certain number of cycles. However, this basic assumption is difficult to verify by experiments on cyclic loading, because the onset of the ratcheting with the increase of the loading amplitude is gradual and not sharply defined [28]. This has motivated the development of the bounding surface model, where the elastic regime is shrunk to the current stress point [29].

The other approach to model soil behavior is the *black box* approach, in which the constitutive relation is derived by exploiting mathematical symmetries and representation theorems [30,31]. The main advantage of this approach is that it offers a rigorous mathematical framework for the development of the tensor structure of constitutive relationships. Taking this perspective, some cyclic loading models have been developed starting from the theory of hypoplasticity [30]. This theory involves non-linear rate terms in order to capture the typical loading-unloading behavior of plastic deformation. Besides the stress and the void ratio, hypoplastic models introduce additional internal variables such as the back stress tensor [32] or the intergranular strain [33]. In order to give a physical basis to these internal variables, the concept of granular temperature has been introduced as a measure for velocity fluctuations of the grains [1,34,35]. However, the range of validity of statistical mechanics used in these approaches is still not fully resolved.

1.3 Micromechanical modeling

Most of the attempts to identify the internal variables of constitutive equations are based on macromechanical observations of the response of soil samples in conventional apparatus. A micromechanical investigation would help to select the physically motivated internal variables and to get insight into the principles and mechanics determining their evolution. After all, the mechanical response of granular soils is no more than a combined response of many micromechanical arrangements, such as interparticle slips, breakage of grains

and wearing of the contacts. The development of micromechanical constitutive models is specially motivated by recent experiments on granular materials at grain scale [36]. Using photoelastic disks, these experiments show that stress in granular materials is transmitted through an heterogeneous contact network which reflects a broad contact force distribution. This broadness leads in turn to a considerable number of sliding contacts. These contacts are defined by the condition $|f_t| = \mu f_n$, where f_n and f_t are the normal and tangential contact force and μ the coefficient of friction. Under small deviatoric loads, an initially isotropic packing develops an anisotropic contact network because new contacts are created along the loading direction, while some contacts are lost perpendicular to it [36–38]. Anisotropy is also observed in the subnetwork of sliding contacts, because some contacts leave the sliding condition under slight deviatoric loading [39]. Geometrical anisotropy leads to an anisotropic response of the granular assembly. The effect of the anisotropy of the contact network on the elastoplastic response has been recently investigated by the introduction of fabric tensors, measuring the orientational distribution of the contacts [39].

The investigation of granular soils using particle-based simulations often involves oversimplified particle geometries and contacts laws which are far from the properties of real soils. Nevertheless, these models are useful for identifying the role of induced anisotropy and the emergence of force chains in the elastoplastic response of these materials [40,41]. Despite their simplicity, particle-based models reproduce the complex structure of the incremental stress-strain response of granular materials [42,40,43,44]. These findings support attempts to base the construction of macroscopic constitutive relations on particle-based models. The particle models should capture realistic granulometric properties and interparticles interactions, and the constitutive models will describe the response of these particle models using incremental (or rate type) relations. The incremental relation can then be used in the Finite Element Codes for large scale simulations.

The method of calculating the incremental response of particle-based models is the same as used soil mechanics [46,47]. This method has been implemented to calculate the incremental response of packings of disks [42] and polygons [45,39]. The incremental response in three-dimensional deformations has also been investigated using packings of spheres [43,44]. However, most of these calculations are still confined to plane strain deformation. In this case the stress space is completely described by the volumetric (p) and deviatoric (q) components of the stress. The incremental strain defines the strain space, whose components are the volumetric (de) and deviatoric ($d\gamma$) strain.The noncoaxiality angle, measuring the orientation of the principal direction of the strain with respect to the principal direction of the stress, is required for anisotropic materials [39]. The incremental response is given by a function between the incremental stress space and the incremental strain space.

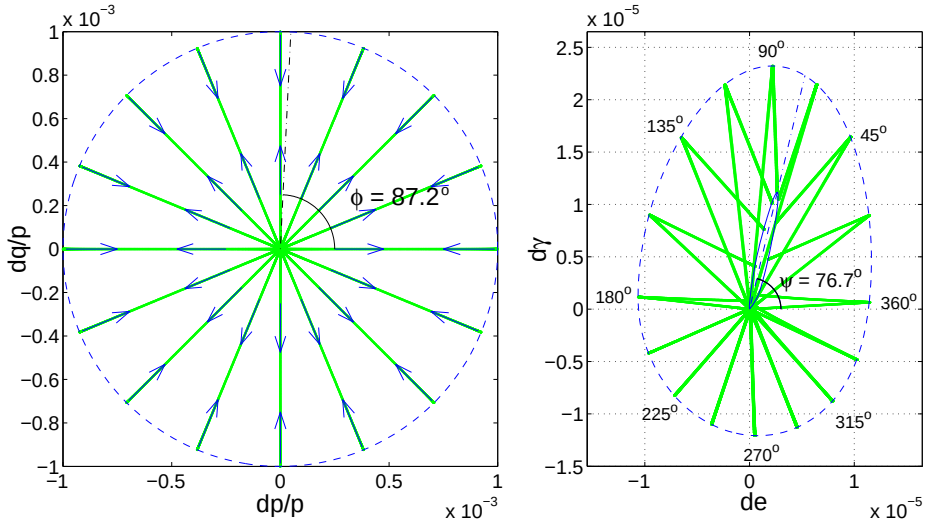

Fig. 2. Stress - strain relation resulting from the load - unload tests using a packing of polygons [45]. The stress components are the pressure $p = (\sigma_1 + \sigma_2)/2$ and the deviatoric stress $q = (\sigma_1 - \sigma_2)/2$. σ_1 and σ_2 are the principal components of the stress. The strain components are given by the volumetric de and the deviatoric $d\gamma$ part of the strain tensor. Grey solid lines are the paths in the stress and strain spaces. Grey dash-dotted lines represent the yield direction (left) and the flow direction (right). Dashed line shows the strain envelope response and the solid line is the plastic envelope response.The components of the initial stress state are $\sigma_1 = 1.25 \times 10^{-3} k_n$ and $\sigma_2 = 0.75 \times 10^{-3} k_n$. Here k_n is the normal stiffness at the contacts.

Fig. 2 shows the typical incremental response resulting from a simulation using a perfect polygonal packing [45]. Starting from a point in the stress space, the packing is loaded using a specific direction and a fixed loading amplitude $\Delta\sigma = \sqrt{p^2 + q^2}$. The end of the load paths in the stress space maps into a strain envelope response in the strain space. Then the sample is unloaded so that the sample returns to its original stress state. The corresponding strain point does not return to its initial state, so that the remaining strain corresponds to the plastic incremental strain. This procedure is implemented by choosing different stress directions with the same stress amplitude, so that the ends of the strain paths create the plastic part of the envelope response. As shown in Fig. 2, this envelope consists of a very thin ellipse, nearly a straight line, which confirms the unidirectional aspect of the irreversible response predicted by the elastoplasticity theory [48]. The *yield direction* ϕ can be found from this response, as the direction in the stress space where the plastic response is maximal. In this example, this is around $\phi = 87.2°$. The *flow direction* ψ is given by the direction of the maximal plastic response in the strain space, which is around 76.7°. The fact that these directions do not agree reflects a *non-associated flow rule*, that is also observed in experiments on realistic soils [46]. From numerical simulations of packings of disks, Bardet concluded also that a non-associated flow rule describes satisfactorily the incremental response [42]. This conclusion is also supported by several experimental tests on

plane strain deformation [48,52,22]. Both numerical and experimental results show clearly deviations from the normality condition. A possible reason for these deviations is that any load involves sliding contacts, so that the elastic regime is vanishing small, not a finite domain as the Classical Elastoplasticity assumes [40]. These results lead to the conclusion that a profound modification of elastoplasticity theory is required [49].

Apart from the unidirectionality of the flow rule, simulations show that the dilatancy $d = -de^p/d\gamma^p$ and the stress ratio $\eta = q/p$ are related by the simple linear relation $d = c(\eta - M)$ (Fig. 3) [39]. This relation is not only supported by experiments, but it also has been one of the fundamental issues in modeling the stress-strain behavior of soils [50]. A physical explanation of this relation is that the granular sample behaves like a *strange fluid*, that obeys this stress-dilatancy relation as an internal kinematic constraint [51]. This constraint becomes apparent near failure, where the plastic deformation dominates, and it could be seen as the counterpart of the well-known incompressibility condition of fluids. In this context, we should address the existing correlation between the mean orientation of the sliding contacts and the plastic flow direction [39]. This correlation suggests that this internal constraint can be micromechanically interpreted from the induced anisotropy of the sub-network of sliding contacts.

In the limit of small deviatoric loads, the kinematic constraint is not longer valid because elastic deformation dominates. However, the correlation between the stress-dilatancy relationship and the induced anisotropy is still valid [39]. Under extremely small deviatoric loads, some contacts depart from the sliding condition, leading in turn to an anisotropy in the subnetwork of the sliding contacts. The effect of this anisotropy on the plastic response becomes evident when we get the plastic envelope response of an isotropically compressed sample, see Fig. 3. Unexpectedly, the unidirectionality of the plastic deformations breaks down, because small deviatoric loads lead to deviatoric plastic deformations. This surprising effect contradicts the isotropic regimen postulated in several constitutive models [52].

We will study here how this plastic deformation evolves when an isotropically compressed sample is subjected to small cycles with deviatoric stress. We will see that the deviatoric strain increases as the number of cycles increases. A very surprising fact is that this accumulation does not stop for large number of cycles, but it grows linearly with respect of the number of cycles. We call his phenomena granular ratcheting.

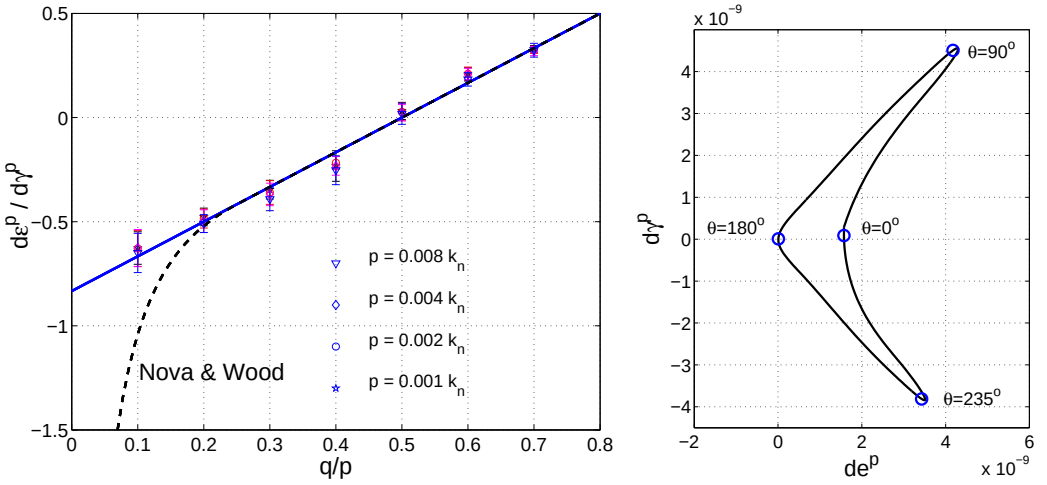

Fig. 3. Left:Dilatancy $d = -de^p/d\gamma^p$ versus the stress ratio $\eta = q/p$ obtained from the plastic incremental response of a polygonal packing [39]. The solid curve represents a linear fit; The dashed curve the relation given by the Nova & Wood model [52]. Right: Plastic envelope response resulting from isotropically compressed polygonal packing with a pressure $p = 0.001k_n$. Here k_n is the normal stiffness at the contacts.

2 Granular ratcheting

We use a particle-based model with polygonal particles to investigate granular ratcheting. The polygons are generated by Voronoi tessellation [45]. This method produces a range of areas of polygons following a Gaussian distribution with mean value ℓ^2 and variance of $0.36\ell^2$. The number of edges of the polygons is distributed between 4 and 8 for 98.7% of the polygons, with a mean value of 6. The interparticle forces include elasticity, viscous damping and friction with a sliding condition. The ratio between the tangential and normal contact stiffnesses is $k_t/k_n = 0.33$, and the friction coefficient is $\mu = 0.25$. The details of this particle model can be found elsewhere [2].

Simulations are performed using five different samples. Each sample consist of 400 polygons, which are packed in the following way: First, the polygons are placed randomly inside a rectangular frame consisting of four walls. Then, a gravitational field is applied and the sample is allowed to consolidate. The external load is imposed by applying a force $\sigma_1 H$ and $\sigma_2 W$ on the horizontal and vertical walls, respectively. Here σ_1 and σ_2 are the vertical and horizontal stresses. H and W are the height and the width of the sample. The polygonal packing is isotropically compressed until the pressure p_0 is reached. When the velocity of the polygons vanishes gravity is switched off. Then, the vertical stress $\sigma_1 = p_0$ is kept constant and horizontal stress is modulated as

$$\sigma_2 = p_0 + \Delta\sigma[1 - \cos(\pi t/t_0)]/2, \tag{1}$$

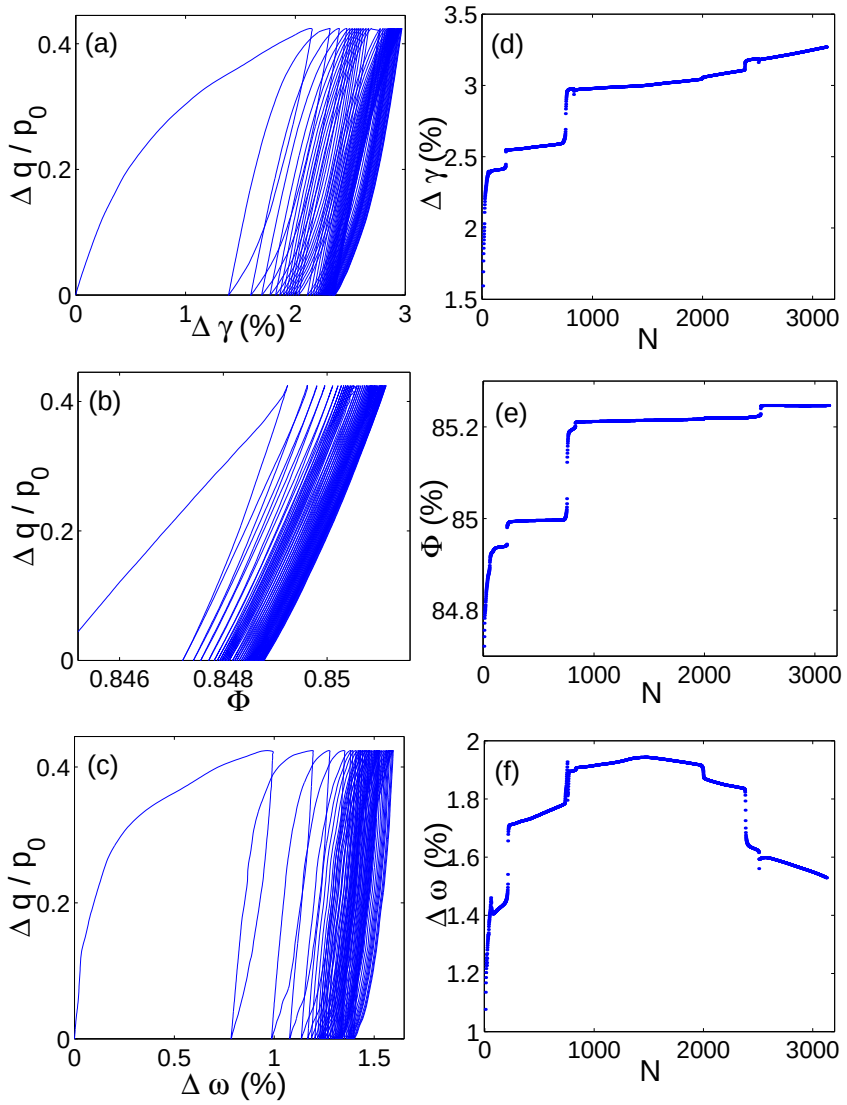

Fig. 4. Stress-deformation relation in a polygonal packing subjected to cyclic loading: (a) Deviatoric stress versus deviatoric strain in the first 40 cycles. (b) Permanent (plastic) strain γ_N after N cycles versus the number of cycles. (c) Stress against the volume fraction in the first 40 cycles. (d) Volume fraction Φ_N after N cycles versus number of cycles.(e) Stress against vorticity $\Delta\omega$. (f) vorticity after N cycles versus number of cycles.

being $\Delta\sigma$ the loading amplitude and t_0 the period of each cycle.

2.1 Stress-strain relation

The strain tensor is calculated as the symmetric part of F_{ij}, where F_{ij} is the average of the gradient of the displacement field over a representative element volume (RVE). This volume consists of the space occupied by all the particles

whose distance from the center of the assembly is less than 10ℓ. The exact expression of the averaged displacement field over the (RVE) can be found in [40]. From the eigenvalues ϵ_1 and ϵ_2 of the symmetric part of the strain tensor we obtain the deviatoric strain as $\gamma = \epsilon_1 - \epsilon_2$. The volume fraction is calculated as $\Phi = (V_p - V_0)/V_b$, where V_p is the sum of the areas of the polygons, V_0 the sum of the overlapping areas between them, and V_b the area of the rectangular box. The vorticity is calculated as the antisymmetric part $\omega = (F_{12} - F_{21})/2$ of F_{ij}.

Part (a) of Fig. 4 shows the relation between the stress $q = (\sigma_1 - \sigma_2)/2$ and the shear strain γ in the case of a loading amplitude $\Delta\sigma = 0.424p_0$. This relation consists of open hysteresis loops which narrow as consecutive load-unload cycles are applied. This hysteresis produces an accumulation of strain with the number of cycles which is represented by γ_N in the part (d) of Fig 4. We observe that γ_N consists of short time regimes, with rapid accumulation of plastic strain, and long time *ratcheting* regimes, with a constant accumulation rate of plastic strain of around 10^{-6} per cycle.

The relation between the stress and the volume fraction is shown in part (b) of Fig. 4. This consists of asymmetric compaction-dilation cycles leading to compaction during cyclic loading. This compaction is shown in part (e) of Fig. 4. We observe a slow variation of the volume fraction during the *ratcheting* regime, and a rapid compaction during the the transition between two ratcheting regimes. The slope of γ_N shows no dependency on the compaction level of the sample. The evolution of the volume fraction seems to be rather sensitive to the initial random structure of the polygons. Even so we found that after 3×10^3 cycles the volume fraction still slowly increases in all the samples, without reaching a saturation level.

Vortices contribute substantially to global deformation, as shown the Part (c) of Fig. 4. We observe clockwise vorticity in the loading stage, followed by counterclockwise vorticity in the unloading stage. Vorticity also changes drastically during the transition between two ratcheting regimes, as shown Part (f) of Fig. 4. The vorticity evolves slowly during ratcheting regimes; and rapidly during the transition between two ratcheting regimes. A non-monotonic behavior is observed in the time evolution of this vorticity field. This behavior is not affected by the compactification level of the sample.

One would expect that for small enough loading amplitudes, one can reach the elastic regime postulated in the shakedown theory [25]. In an attempt to detect this elastic regime, we decreased the amplitude of the load cycles and evaluated the corresponding asymptotic response of the deviatoric plastic strain. During the first cycles a transient regime showing a decay of the permanent deformation per cycle is observed. However, after some hundred cycles, the sample reaches an asymptotic limit, where the plastic deformation in each

cycle becomes constant. Regardless of the amplitude of the loading cycles, one always obtains ratcheting behavior in the long time limit. This is shown in the accumulation strain rate $\Delta\gamma/\Delta N$ for different loading amplitudes $\Delta\sigma$ in Fig. 5. A constant accumulation of strain is observed during cyclic loading, even when the amplitude is as small as 10^{-3} times the applied pressure. Of course, due the smallness of the ratcheting response for these loading amplitudes, one can say that for small loading amplitudes the response is practically elastic. Even if the slight repeated loading produced by transit of ants would produce plastic deformation after some centuries, it is not possible to make them to follow the same path all this time. However, it is important to note that Fig. 5 shows a smooth transition from the shakedown response to the ratcheting response. This means that the transition from ratcheting to shakedown regime is too smooth that it does not allow identification of a purely elastic regime.

In view of the extremely small strain levels accumulated during the cycling loading, one would doubt that the simulations really capture the physical origin of the phenomenon. In this respect, we should point out that the results do not change nor when the time step is decreased neither when the floating point precision is increased. Therefore we have no reason to believe that the ratcheting comes from a cumulative systematic error of the numerical method.

Another important question is whether ratcheting is a genuine quasistatic effect. Since the equations of motion include damping forces and inertia terms, it is important to know their role in granular ratcheting. Damping and inertial effects can be evaluated by performing the same test with different loading frequencies. Fig. 6 shows that as the frequency is reduced, the ratcheting tends to a constant value. From this result one can conclude that damping or inertial effects do not affect the appearance of ratcheting in the sample, so that this is a purely quasistatic effect.

3 Micromechanics of granular ratcheting

The existence of ratcheting for extremely small loading amplitudes appears to be somewhat counter-intuitive. First, from the classical theory of elastoplasticity one would expect a certain regime where only reversible deformation is possible. Second, our discrete model does not incorporate wearing of the grains. In practice, abrasion at the contacts leads to progressive rounding of the grains, which explains the accumulation of plastic deformation under cyclic loading [53]. Nevertheless, we will see that the dynamics of the contact network can explain how ratcheting evolves in samples with constant granulometrical properties.

Each contact is characterized by the variables shown in Fig. 7. The contact

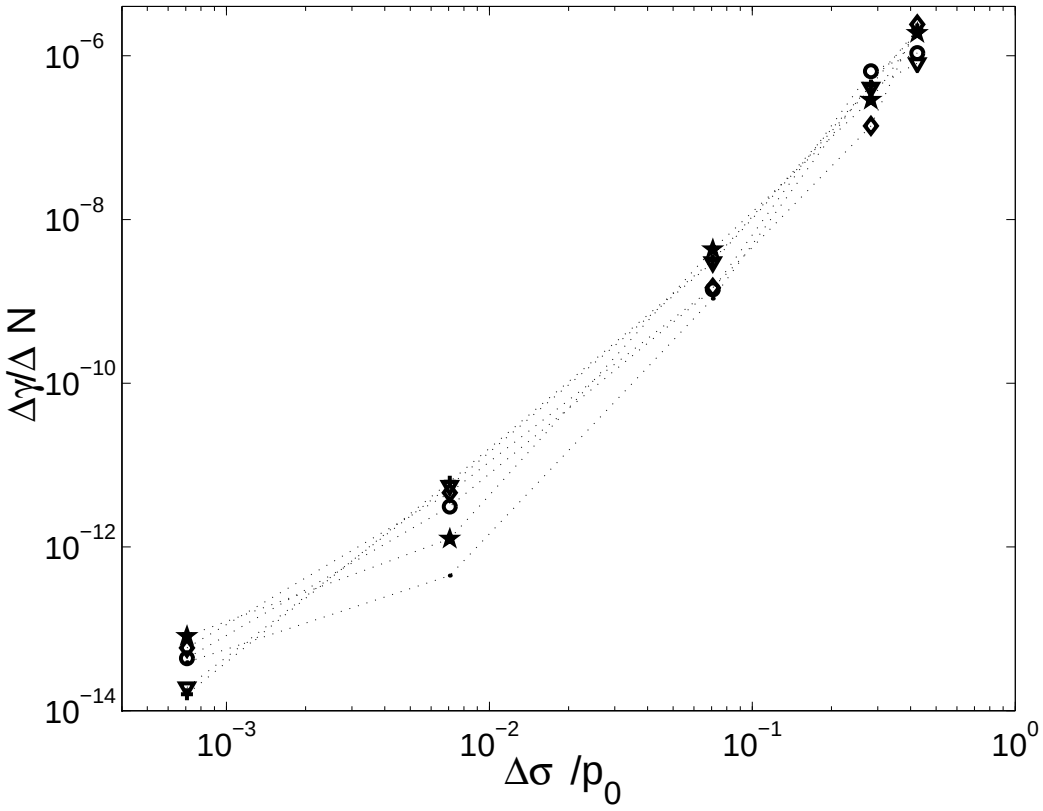

Fig. 5. Permanent deviatoric deformation per cycle versus loading amplitude in the ratcheting regime. The calculations are performed on six different polygonal samples [2].

force $\vec{f}$ is decomposed into its normal f_n and tangential f_t components with respect to the contact surface. The angle φ is the orientation of the normal force. The mobilized angle $\eta = \arctan(f_t/f_n)$ allows us to distinguish between sliding and non sliding contacts. The sliding condition is given by $\tan(\eta) = \pm\mu$, where μ is the coefficient of friction.

3.1 Contact network

A striking feature of granular materials is the convoluted heterogeneous structure of the contact forces. As shown in Fig. 8, The stress applied on the boundary of the assembly is transmitted through force chains along which the contact forces are stronger than on average. Force chains lead to a wide distribution of the contact forces in both the tangential and normal directions.

We first study the evolution of the distribution of the normal forces f_n and mobilized angle η during cyclic loading. A broadening of the distribution is observed during each loading phase, followed by a narrowing of the distribution during the unloading phase. When the ratcheting regime is reached, the time

evolution of this distribution is characterized by a broadening phase followed by a narrowing one in each cycle. In the ratcheting regime, this distribution show a periodic broadening-narrowing regime.

To demonstrate this periodicity, the distribution of normal forces and mobilized angles at different snapshots of the simulation is plotted in Figure 9. Note that although all distributions were measured at different times of the simulation, they correspond to the same stage of the cyclic loading. The shape of the distribution at this point remains approximately constant throughout the whole simulation. The contact force distribution evolves almost periodically during the cyclic loading. We also observe a peak in the distribution of mobilized angle at $\eta = \mu = 0.25$. This peak suggests that an important number of contacts reach periodically the sliding condition during the ratcheting regime. An important issue in the granular ratcheting is the orientational distribution of these sliding contacts, which is studied in the next section.

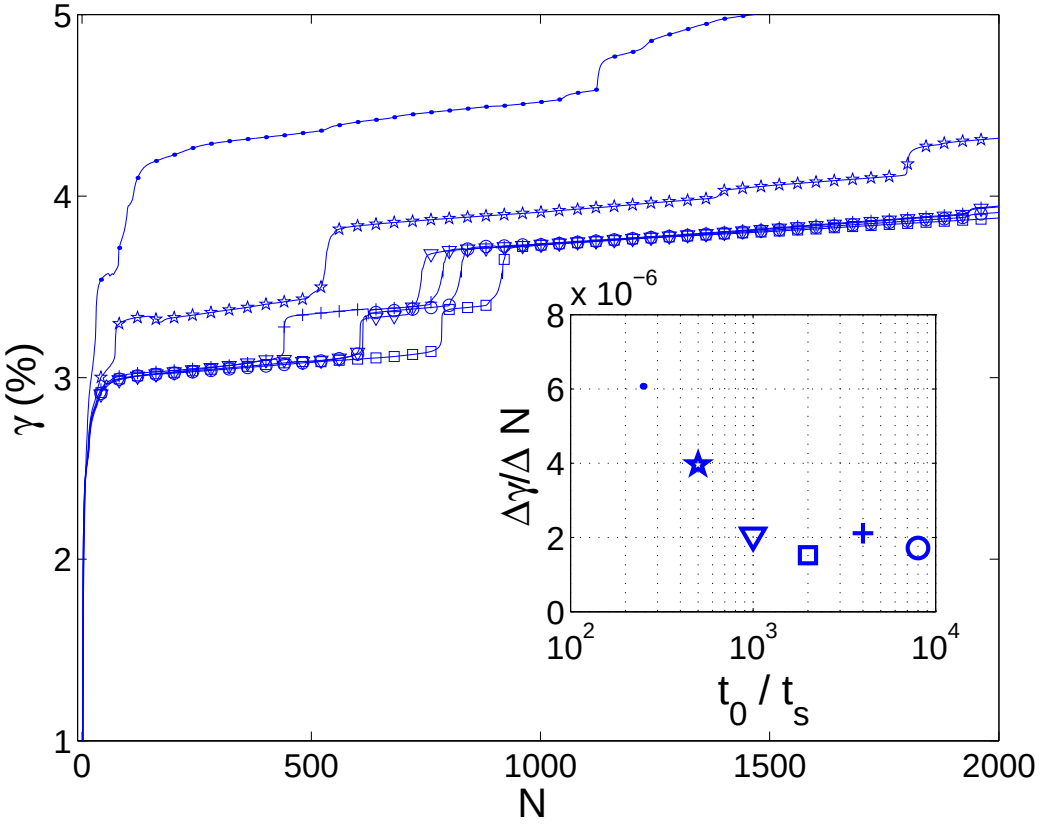

Fig. 6. Permanent deviatoric strain versus the number of cycles for different periods of cyclic loading t_0. The inset shows the plastic deformation per cycle averaged over the last 1000 cycles. Each symbol in the inset corresponds to a value of t_0/t_s, where $t_s = \sqrt{m/k_n}$, m being the averaged mass of the polygons, and t_0 is defined in Eq. 1.

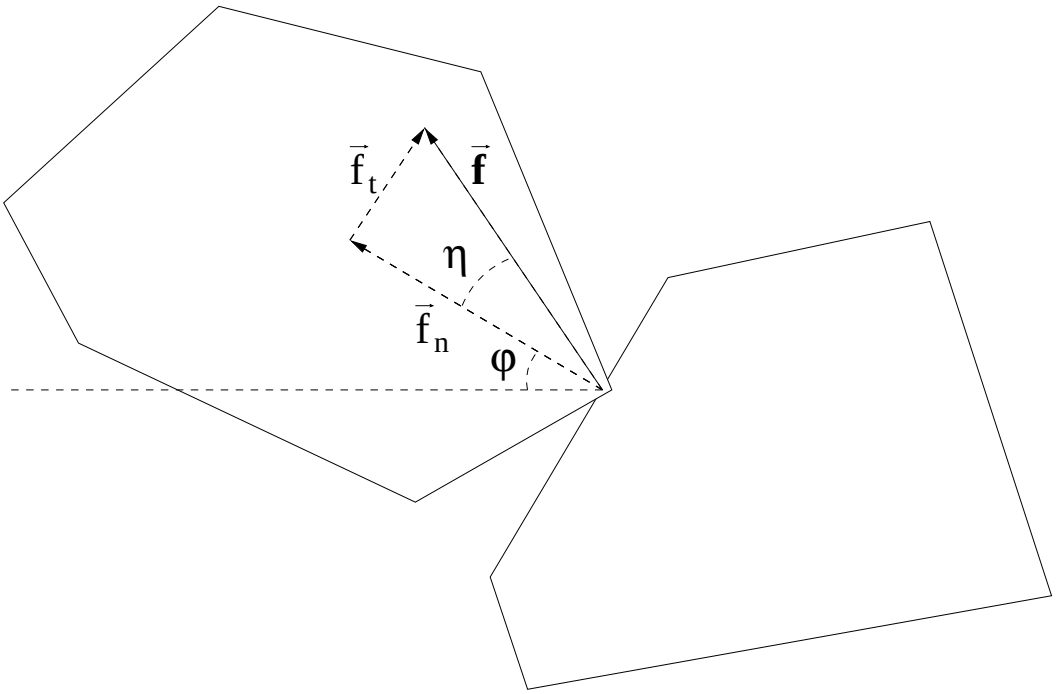

Fig. 7. Relevant variables of the contact force $\vec{f}$. This is decomposed into a normal $\vec{f_n}$ and a tangential $\vec{f_t}$ component. The orientation angle φ is the direction of the normal force. The mobilized angle η satisfies $\eta = \arctan(f_t/f_n)$.

3.2 Anisotropy of the sliding contacts

The anisotropy of the granular sample can be characterized by the orientational distribution of the normal forces. For small deviatoric loads (i. e.

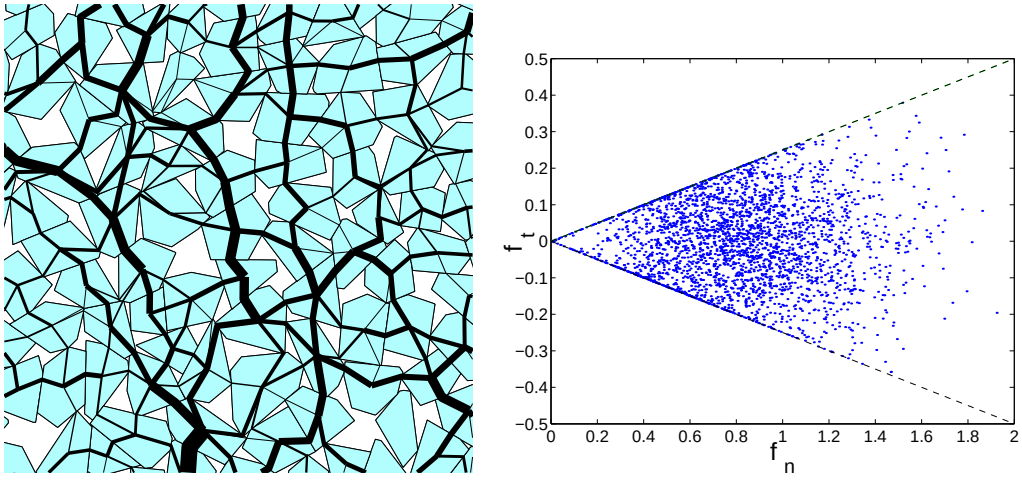

Fig. 8. Left:Contact force network in an isotropically compressed sample. The width of the lines represents the size of the normal force. Right:Distribution of contact forces. Each point represents the normal and tangential component of the contact force. Dashed lines represent the sliding condition $|f_t| = \mu f_n$.

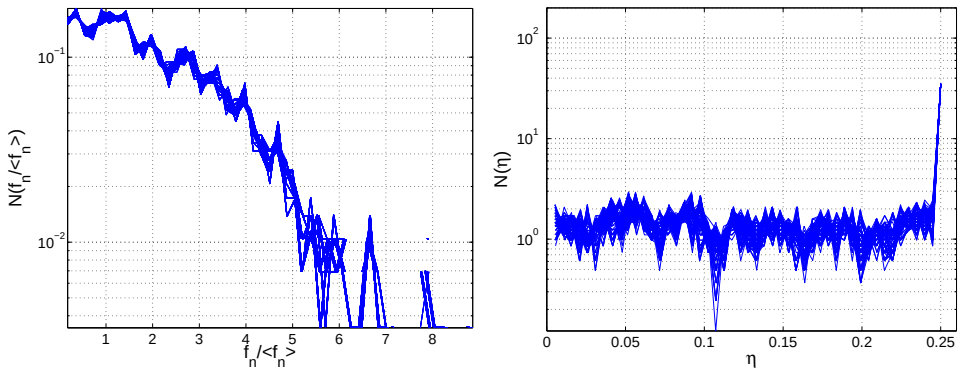

Fig. 9. Distribution function of the normal forces (Left) and mobilized angle (Right) at the contacts. The distributions are calculated from different times during the ratcheting regime ($time = Nt_0$, where $N = 1000, 1001...1500$). The frequency distributions are constructed by segmenting the range of the data into 100 equal sized bins.

$\Delta\sigma < 0.5\Delta\sigma_{max}$, where $\Delta\sigma_{max}$ is the peak value), anisotropy in the contact network is almost absent, and the coordination number of the packing keeps approximately its initial value $N_0 \approx 4.4$ in all the simulations.

The onset of anisotropy is different if one considers only the sliding contacts. These contacts play an important role, because they carry most of the irreversible deformation of the granular assembly during the cyclic loading. This anisotropy is described by the polar function $\Omega^s(\varphi)$, where $\Omega^s(\varphi)\Delta\varphi$ is the number of sliding contacts per particle whose normal force is oriented between φ and $\varphi + \Delta\varphi$.

Samples compressed with zero deviatoric load are characterized by an isotropic distribution of sliding contacts. However, this isotropy is broken when the sample is subjected to the slightest deviatoric load. This appearance of the anisotropy can be schematically explained from Fig. 7. Let us assume that the contact force satisfies the sliding condition $f_t = \mu f_n$. Imagine that a small loading is imposed on the assembly in the vertical direction. If the normal component of the force is parallel to the loading direction, this component tends to increases more than the tangential force, so that the contact is likely to leave the sliding condition. On the contrary, if the tangential force is parallel to the loading direction it increases more than the normal force, and the contact is likely to remain in the sliding condition.

This picture is useful for explaining the complex evolution of the orientational distribution of the sliding contacts shown in Fig. 10. During the first cycle, sliding contacts whose normal force is oriented nearly parallel to the load direction leave the sliding condition during the loading phase, and some of them slip during the unload phase. On the other hand, the sliding contacts whose normal force is orientated nearly perpendicular to the load direction slip during the loading phase, and leave the sliding condition during the unload

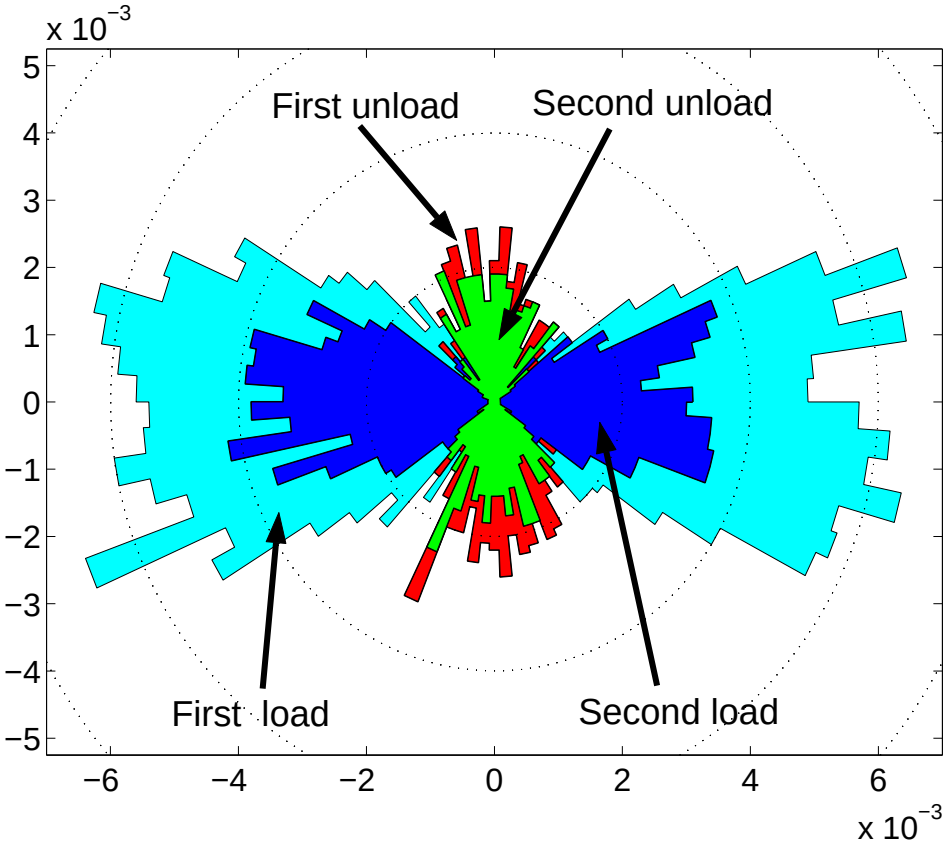

Fig. 10. Distribution of the orientation φ of the contacts reaching the sliding condition during the first two load-unload phases

phase. In the first approximation, the anisotropy can be given by

$$\Omega^s(\varphi) \approx \begin{cases} \frac{N_0 n_s}{2\pi}(1-\cos(2\varphi)) & : \quad \textit{loading phase}, \\ \frac{N_0 n_s}{2\pi}(1-\sin(2\varphi)) & : \quad \textit{unloading phase}, \end{cases} \tag{2}$$

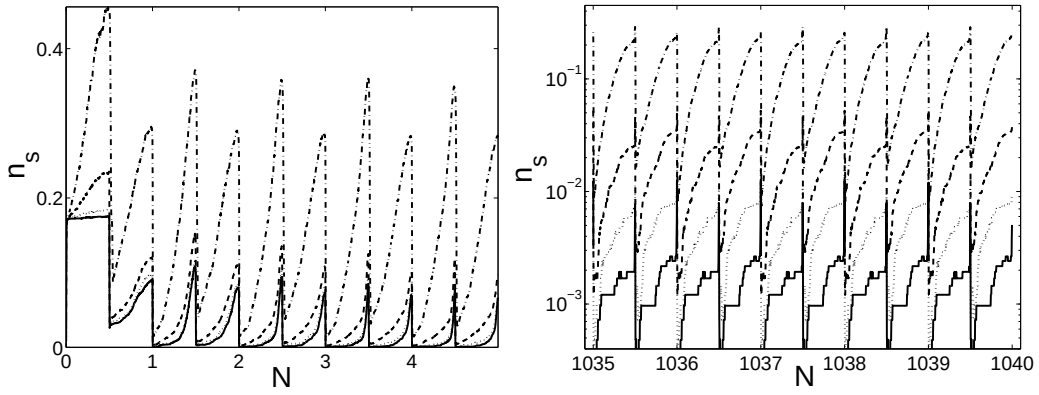

Fig. 11. Fraction of sliding contacts n_s in the short (left) and long time (right) behavior for different values of $\Delta\sigma_y/p_0$: 0.424 (dash-dotted line), 0.0707 (dashed line), 0.00707 (dotted line) and 0.000707 (solid line)[2]

where $N_0 \approx 4.4$ is the averaged number of coordination number and n_s the fraction of sliding contacts. This description uses a single fabric coefficient n_s, which is accurate for intermediate loading amplitudes. For small loads the approximation is questionable due to the scarce number of sliding contacts. For large loads, an significant number of contacts reach the sliding contacts in both the load and unload phase, so that higher order fabric coefficients are required [40]. However, n_s can be consider as the most important internal variable describing the cyclic loading response.

The time evolution of n_s during cyclic loading is shown in Fig 11. The relevance of this variable is demonstrated if one compares it with the evolution of the stiffness of the material. The latter is given by the slope of the stress strain curve in part (a) of Fig. 4. During each loading phase, the number of sliding contacts increases, giving rise to a continuous decrease of the stiffness as shown in part (a) of Fig. 4. The abrupt reduction in the number of sliding contacts at the transition from load to unload is reflected by the typical discontinuity in the stiffness observed under reversal loading. During cyclic loading the number of sliding contacts tends to decrease, which produces a narrowing of the hysteresis loops. In the long time behavior one can also see that some contacts reach almost periodically the sliding state even for extremely small loading cycles, leading to a constant amount of plastic deformation per cycle. Note also that the number of contacts reaching the sliding conditions is almost the same in both loading and unloading phase. This makes the hysteresis loop almost symmetric, but slightly open to allow accumulation of plastic deformation.

At the contact level, the constant plastic deformation per cycle is explained from the variation of both force and displacement at the contacts. Parts (a) and (c) of Fig. 12 show the trajectory of the normal and tangential components of the force for two sliding contacts. After a certain number of loading cycles, the contact forces reach a periodic regime, some of them reaching periodically the sliding condition. The load-unload asymmetry of the contact force loop, producing a slip at the contact of the same amount and in the same direction during each loading cycle.

A measure for the plastic deformation of the sliding contact is given by $\xi = (\Delta x_t^c - \Delta x_t^e)/\ell$, where Δx_t^c and Δx_t^e are the total and the elastic part of the tangential displacement at the contact. Parts (b) and (d) of Fig. 12 show the plastic deformation ξ of the two sliding contacts. Due to the load-unload asymmetry of the contact force loop, a net accumulation of plastic deformation is observed in each cycle. In the case of the contact shown in part (b) of Fig. 12, the contact slips forward during the loading, and backward during the unloading phase. This sliding results in a net accumulation of permanent deformation per cycle. The other contact behaves elastically during the loading and slips during the unloading. This mechanism resembles the

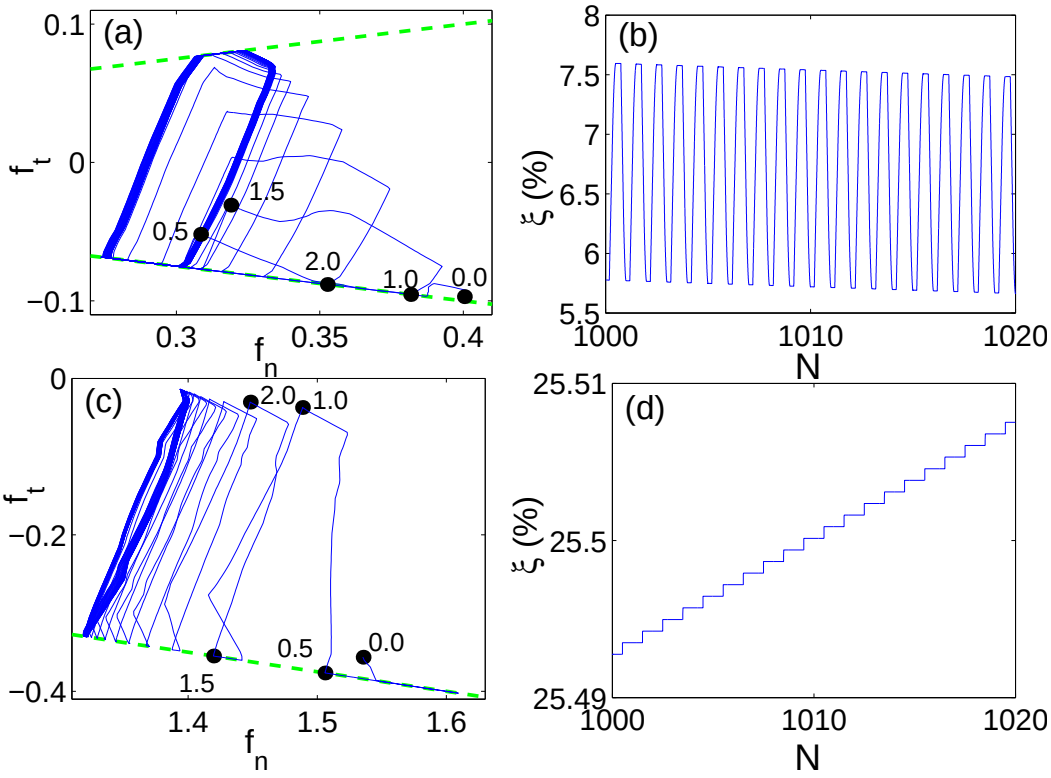

Fig. 12. (a) and (b) Trajectories of the contact force of two selected sliding contacts. The dots denote the times $t = 0, 0.5t_0, ..., 2t_0$, where t_0 is the period of the cyclic loading. The dashed line shows the sliding condition $|f_t| = \mu f_n$. (b) and (d) Plastic deformation ξ at the contacts shown in (a) and (c).

ratchets devices presented in Sec.1.1. That is why this phenomenon is called granular ratcheting.

3.3 Displacement field

During the ratcheting regime, there is a constant accumulation of plastic deformation per cycle at each one of the sliding contacts. An immediate consequence of this fact is that each particle within the packing has a certain displacement and accumulates the same rotation for each cycle. The typical displacement of one particle during the cyclic loading is shown in Fig. 13. During the ratcheting regime, the particle moves the same amount in each cycle. This displacement remains constant during the long time of a ratcheting regime, but it changes abruptly during the transition between two ratcheting regimes. Typically, the maximal displacement per cycle at this transition is one or two orders of magnitude larger than in the ratcheting regimes. Therefore most of the deformation in the granular assembly occurs during the transitions. Deformation during ratcheting is relative small, but is sufficient to drive the system to unstable stages with relative large deformation.

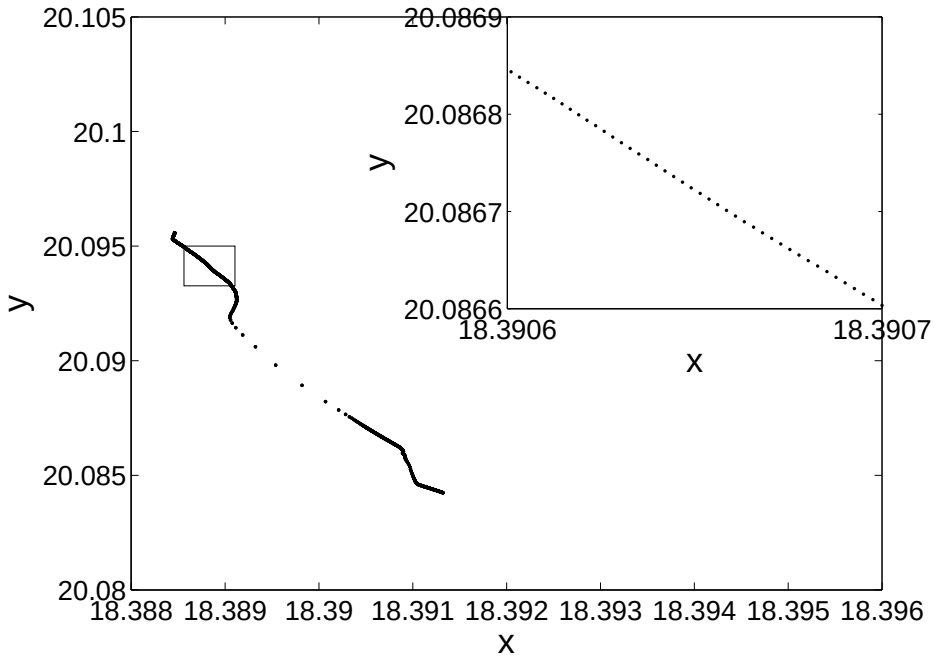

Fig. 13. Position of a single particle after each cycle. The detail shows the displacement during the ratcheting regime.

It is interesting to observe the spatial correlation of such particle displacements. The most interesting deformation patterns is the formation of vorticity cells, see Fig. 14. Slow vorticity motion appears during the ratcheting regime, and fast motion vortices appears during the transition between two ratcheting regimes. This explains the evolution of the vorticity shown in part (c) of the Fig. 4, as well as the abrupt changes of vorticity shown in part (f) of Fig. 4

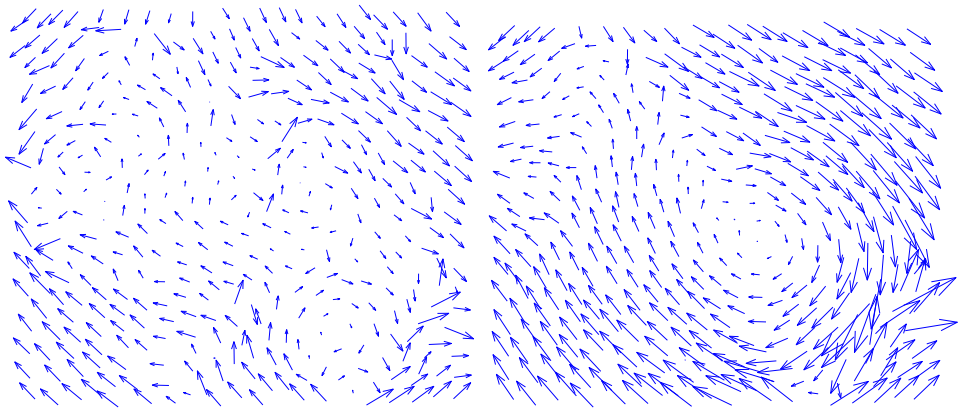

Fig. 14. Displacement field during one loading cycle. The load amplitude is $\Delta\sigma = 0.6p_0$, and $p_0 = 0.001k_n$. The left image corresponds to the displacement per cycle during the ratcheting regime; the right one is the displacement per cycle during the transition between two ratcheting regimes. The arrows represent $10^5\Delta\vec{u}$ in the left image and $10^3\Delta\vec{u}$ in the right one, where $\Delta\vec{u}$ is the displacement of the particle per cycle.

Vortex structures are created and destroyed during the transitions. Therefore the vorticity patterns in each ratcheting regime is completely different from the previous one.

Since the vorticity is linked with the a non-vanishing antisymmetric part of the displacement gradient, the strain tensor is not sufficient to provide a complete description of this convective motion during cyclic loading. Slip zones and rotational bearings are other persistent deformation patterns during the cyclic loading [2,6]. They appear periodically during each ratcheting regime. Patterns are destroyed and new ones are created during the transition between two ratcheting regimes. An appropriate constitutive model for ratcheting demands additional degrees of freedom in the continuum, taking into account these deformation patterns in strain-like variables.

4 Concluding remarks

A grain scale investigation of the cyclic loading response of a packing of polygons has been presented. In the quasistatic limit, we have shown the existence of long time regimes with a constant accumulation of plastic deformation per cycle, due to ratchet-like motion at the sliding contacts. As the loading amplitude decreases, a smooth transition from ratcheting to shakedown is observed, which does not allow one to identify a purely elastic regime.

The overall response of the polygonal packing under cyclic loading consists of a sequence of long time ratcheting regimes, with slow accumulation of plastic deformation in terms of deviatoric strains, compaction and vorticity. These regimes are separated by short time regimes with large plastic deformations. The analysis of the displacement field per cycle of the particles shows that cyclic loading induce convective motion inside the sample. These motion appears in form of vortex-like structures, which persist during the ratcheting regime.

The existence of granular ratcheting may have deep implications in the study of permanent deformation of geomaterials subject to cyclic loading. More precisely, the classical concept of an elastic regime needs to be abandoned, because any load induces irreversible deformation. A continuum description of ratcheting requires the introduction of additional degrees of freedom in the kinematics, as well as internal variables in the constitutive relations. These internal variables must account for the dissipation produced by the sliding contacts in the ratcheting regime, and the restructuring of the granular skeleton during the transition between two ratcheting regimes. Recently two approaches has been suggested to this issue: They extrapolate the statistical mechanics of viscoelastic fluids [35] and thermally activated dislocations [34,54] to jammed

granular materials. These approaches introduce two different temperatures as internal variables, accounting frictional dissipation and energy released by unjammed transitions. The validity of these approaches remains conditioned to the validation of the ergodic hypothesis for jammed granular media.

Geotechnical application of cyclic loading simulations is still limited by the computer time needed for simulations. However, simulations of thousands of cycles with small number of particles can be used to investigate the microscopic origin of granular ratcheting, which will contribute to the development of large scale simulation models. At this time, the similarity of results with the recently reported ratcheting regime in packings of disks [6] and spheres [4] indicates that this effect does not depend on the geometry of the grains, and that it may be inherent to the particle interactions.

Modeling interactions between polygons still poses serious limitations, because of the difficulty to derive conservative elastic forces: When forces between polygons are calculated as a function of their overlapping area, the energy conservation is not guaranteed [55]. An alternative approach is to define the potential energy as a function of overlap, and derive from this potential contact forces and torques [55]. However, this approach leads to unrealistic interactions, because the magnitudes of the torque applied to each particle are the same. Moreover, the derivation of forces from this potential leads to complicated expressions which are difficult to code. A simpler approach has been proposed, where a potential energy is associated to each vertex-edge interaction between the polygons [56]. Mc Namara et al. show further difficulties when the classical Cundall-Strack frictional force is used in simulations of packing of disks [57]. This force leads to path dependency in the potential energy, even when sliding is hindered in the simulations. They also show that alternative methods for calculating tangential forces in packing of disks removes granular ratcheting. Thus, future modeling of cyclic loading needs to develop more realistic normal and tangential contact force laws, and to understand the relation between the contact model and the onset of permanent deformations.

F. Alonso-Marroquin is the recipient of an Australian Research Council Postdoctoral Fellowship (project number DP0772409), and acknowledges the support of the ALERT Geomaterials Prize 2006. The authors thank S. McNamara for discussions, and G. Gudehus for helpful written communications.

References

[1] G. Gudehus, Seismo-hypoplasticity with a granular temperature, Granular Matter 8 (2006) 93–102.

[2] F. Alonso-Marroquin, H. J. Herrmann, Ratcheting of granular materials, Phys.

Rev. Lett. 92 (5) (2004) 054301.

[3] R. Garcia-Rojo, H. J. Herrmann, Shakedown of unbound granular materials, Granular Matter 7 (2) (2005) 109–118.

[4] C. T. David, R. García-Rojo, H. J. Herrmann, S. Luding, Hysteresis and creep in powders and grains, in: R. Garcia-Rojo, H. Herrmann, S. McNamara (Eds.), Proceedings of Powders and Grains 2005, Balkema, Leiden, 2005, pp. 291–294.

[5] A. A. Peña, A. Lizcano, F. Alonso-Marroquin, H. J. Herrmann, Investigation of the asymptotic states of granular materials using a discrete model of anisotropic particles, in: Proceedings of Powders and Grains 2005, Vol. 1, Balkema, 2005, pp. 697–700.

[6] R. García-Rojo, F. Alonso-Marroquin, H. J. Herrmann, Characterization of the material response in the granular ratcheting, Phys. Revi. E 72 (2005) 041302.

[7] T. Triantafyllidis (Ed.), Cyclic Behaviour of Soils and Liquefaction Phenomena, A.A. Balkema Publishers, Leiden, 2004.

[8] F. Lekarp, A. Dawson, U. Isacsson, Permanent strain response of unbound aggregates, J. Transp. Engrg. 126 (1) (2000) 76–82.

[9] R. P. Feynman, R. B. Leighton, M. Sands, The Feynman Lectures on Physics, Vol. 1, Addison - Wesley, Massachusetts, 1963, Ch. 46, pp. 46.1–46.9.

[10] I. Zapata, R. Bartussek, F. Sols, P. Hänggi, Voltage rectification by a squid ratchet, Phys. Rev. Lett. 77 (11) (1996) 2293.

[11] J. Howard, Molecular motors: Structural adaptation to cellular functions, Nature 389 (1997) 561.

[12] P. Reimann, Brownian motors: Noisy transport far from equilibrium, Phys. Rep. 361 (2002) 57.

[13] K. Svoboda, C. F. Schmidt, B. J. Schnapp, S. M. Block, Direct observation of kinesin stepping by optical trapping interferometry, Nature 365 (6448) (1993) 721–727.

[14] K. Kitamura, K. Tokunaga, M. Iwane, T. Yanagida, A single myosin head moves along an actin filament with regular steps of 5.3 nanometres, Nature 397 (1999) 129–134.

[15] P. H. Dybvig, Dusenberry's racheting of consumption: Optimal dynamic consumption and investment given intolerance for any decline in standard of living, The Review of Economic Studies 62 (2) (1995) 287–313.

[16] G. Royer-Carfagni, Granular decohesion thermal damage in marble monuments, in: Novel approaches in civil engineering, Springer-Verlag, Berlin, 2004, pp. 177–185.

[17] M. Huang, Z. Suo, Q. Ma, H. Fujimoto, Thin film cracking and ratcheting caused by temperature cycling, J. Mater. Res. 15 (6) (2000) 1239–1242.

[18] G. L. England, T. D. C. M. Tsang, N. Mihajlovic, J. B. Bazaz, Ratcheting flow of granular materials, in: M. D. Evans, R. J. Fragaszy (Eds.), Static and Dynamic Properties of Gravelly Soils, ASCE, 1995, pp. 64–76.

[19] J. Burland, C. Viggiani, Observazioni sul comportamento della torre di pisa, Rivista Italiana di Geotecnica 28 (3) (1994) 179–200.

[20] S. Lobo-Guerrero, L. E. Vallejo, Discrete element method analysis of railtrack ballast degradation during cyclic loading, Granular Matter 8 (3-4) (2006) 195–204.

[21] K. H. Roscoe, J. B. Burland, On the generalized stress-strain behavior of 'wet' clay, in: Engineering Plasticity, Cambridge University Press, Cambridge, 1968, pp. 535–609.

[22] D. M. Wood, Soil behaviour and critical state soil mechanics, ISBN: 0-521-33782-8, Cambridge, 1990.

[23] G. Gudehus, F. Darve, I. Vardoulakis, Constitutive Relations of soils, Balkema, Rotterdam, 1984.

[24] K. Hashiguchi, Z. P. Chen, Elastoplastic constitutive equation of soil with the subloading surface and rotational hardening, Int. J. Numer. Anal. Meth. Geomech. 22 (1998) 197–227.

[25] R. W. Sharp, J. R. Booker, Shakedown of pavements under moving surface loads, Journal of Transportation Engineering 110 (1984) 1–14.

[26] F. Lekarp, A. Dawson, Modelling permanent deformation behaviour of unbound granular materials, Construction and Building Materials 12 (1) (1998) 9–18.

[27] S. Werkmeister, A. R. Dawson, F. Wellner, Permanent deformation behavior of granular materials and the shakedown theory, Journal of Transportation Research Board 1757 (2001) 75–81.

[28] S. Werkmeister, R. Numrich, A. R. Dawson, F. Wellner, Deformation behaviour of granular material under repeated dynamic loading, in: Environmental Geomechanics, Presses Polytechniques et Universitaires Romandes, Monte Verita, 2002.

[29] Y. F. Dafalias, Bounding surface plasticity. I: Mathematical foundation and hypoplassticity, J. of Engng. Mech 112 (9) (1986) 966–987.

[30] D. Kolymbas, Modern Approaches to Plasticity, Elsevier, 1993.

[31] R. Chambon, J. Desrues, W. Hammad, R. Charlier, CLoE, a new rate type constitutive model for geomaterials. Theoretical basis and implementation, Int. J. Anal. Meth. Geomech. 18 (1994) 253–278.

[32] D. Kolymbas, I. Herle, P. A. Wolfferdorff, A hypoplastic constitutive equation with back stress, Int. J. Anal. Meth. Geomech. 19 (1995) 415–446.

[33] A. Niemunis, I. Herle, Hypoplastic model for cohesionless soils with elastic strain range, Int. J. Mech. Cohesive-Frictional Mater. 2 (1996) 279–299.

[34] G. Gudehus, Seismo-hypoplasticity state limits of granular skeletons, J. Stat. Mech. 7 (2006) P07022.

[35] Y. Jiang, M. Liu, From elasticity to hypoplasticity: Dynamics of granular solids, Phys. Rev. Lett.In press, arXiv:0706.1354v1.

[36] T. S. Majmudar, R. P. Behringer, Contact force measurements and stress-induced anisotropy in granular materials, Nature 435 (2005) 47–61.

[37] S. Luding, Micro-macro transition for anisotropic, frictional granular packings, Int. J. Sol. Struct. 41 (2004) 5821–5836.

[38] M. Madadi, O. Tsoungui, M. Lätzel, S. Luding, On the fabric tensor of polydisperse granular media in 2d, Int. J. Sol. Struct. 41 (9-10) (2004) 2563–2580.

[39] F. Alonso-Marroquin, S. Luding, H. Herrmann, I. Vardoulakis, Role of the anisotropy in the elastoplastic response of a polygonal packing, Phys. Rev. E 51 (2005) 051304.

[40] F. Alonso-Marroquin, H. Herrmann, Investigation of the incremental response of soils using a discrete element model, J. of Eng. Math. 52 (2005) 11–34.

[41] A. Pena, A. Lizcano, F. Alonso-Marroquin, H. J. Herrmann, Biaxial test simulations using a packing of polygonal particles, Int. J. Numer. Anal. Meth. Geomech.Iny. J. Numer. Anal. Meth. Geomech.

[42] J. P. Bardet, Numerical simulations of the incremental responses of idealized granular materials, Int. J. Plasticity 10 (1994) 879–908.

[43] F. Calvetti, G. Viggiani, C. Tamagnini, Micromechanical inspection of constitutive modelling, in: Constitutive modelling and analysis of boundary value problems in Geotechnical Engineering, Hevelius Edizioni, Benevento, 2003, pp. 187–216.

[44] Y. Kishino, On the incremental nonlinearity observed in a numerical model for granular media, Italian Geotechnical Journal 3 (2003) 3–12.

[45] F. Alonso-Marroquin, H. J. Herrmann, Calculation of the incremental stress-strain relation of a polygonal packing, Phys. Rev. E 66 (2002) 021301.

[46] H. B. Poorooshasb, I. Holubec, A. N. Sherbourne, Yielding and flow of sand in triaxial compression, Can. Geotech. J. 4 (4) (1967) 277–398.

[47] G. Gudehus, A comparison of some constitutive laws for soils under radially symmetric loading and unloading, Can. Geotech. J. 20 (1979) 502–516.

[48] P. A. Vermeer, A five-constant model unifying well-established concepts, in: Constitutive Relations of soils, Balkema, Rotterdam, 1984, pp. 175–197.

[49] F. Darve, E. Flavigny, M. Meghachou, Yield surfaces and principle of superposition: revisit through incrementally non-linear constitutive relations., International Journal of Plasticity 11 (8) (1995) 927.

[50] I. Vardoulakis, I. O. Georgopoulos, The stress - dilatancy hypothesis revisited: shear - banding related instabilities., Soils & Foundations 45 (2005) 61–76.

[51] I. Vardoulakis, Rigid granular plasticity model and bifurcation in the triaxial test, Acta Mechanica 49 (1983) 57–79.

[52] R. Nova, D. Wood, A constitutive model for sand in triaxial compression, Int. J. Num. Anal. Meth. Geomech. 3 (1979) 277–299.

[53] G. Festag, Experimental investigation on sand under cyclic loading, in: Constitutive and Centrifuge Modelling: two Extremes, Monte Verita, 2003, pp. 269–277.

[54] G. Gudehus, Physical soil mechanics, Springer, Berlin, 2008, Ch. 4.9, iSBN: 978-3-540-36353-8.

[55] T. Poeschel, T. Schwager, Computational Granular dynamics, Springer, Berlin, 2004.

[56] F. Alonso-Marroquin, An efficient algorithm for computing conservative and frictional interaction between two-dimentional, complex-shaped rigid bodies, submitted to Europysical Letters.

[57] S. Mc.Namara, R. Garcia-Rojo, H.J.Herrmann, Microscopic origin of granular ratcheting, submitted to Phys.Rev. E.